Constraining scale-dependent non-Gaussianity with future large-scale structure and the CMB

Adam Becker,[a] **Dragan Huterer**[a] **and Kenji Kadota**[a,b]

[a]Department of Physics and Michigan Center for Theoretical Physics,
University of Michigan,
450 Church Street, Ann Arbor, MI 48109, U.S.A.
[b]Physics Department, Nagoya University,
Nagoya, Aichi 464-8602, Japan

E-mail: beckeram@umich.edu, huterer@umich.edu,
kadota.kenji@f.mbox.nagoya-u.ac.jp

Abstract. We forecast combined future constraints from the cosmic microwave background and large-scale structure on the models of primordial non-Gaussianity. We study the *generalized* local model of non-Gaussianity, where the parameter $f_{\rm NL}$ is promoted to a function of scale, and present the principal component analysis applicable to an arbitrary form of $f_{\rm NL}(k)$. We emphasize the complementarity between the CMB and LSS by using Planck, DES and BigBOSS surveys as examples, forecast constraints on the power-law $f_{\rm NL}(k)$ model, and introduce the figure of merit for measurements of scale-dependent non-Gaussianity.

Contents

1 Introduction

There has recently been a surge in interest to study departures in the distribution of primordial density fluctuations from the random Gaussian case predicted by standard inflationary models. The reason for this renewed interest lies in the fact that any observable departures from Gaussianity would essentially rule out the standard single-field, slow-roll inflationary picture, pointing to a more complicated dynamics during the epoch of inflation (see e.g. [1–5] for reviews).

It is therefore important to consider how one could parametrize primordial non-Gaussianity. A much-studied model of primordial non-Gaussianity is the local (or squeezed) model, which characterizes non-Gaussianity through a single parameter f_{NL} [6–8]

$$\Phi(x) = \phi_G(x) + f_{NL}(\phi_G(x)^2 - \langle\phi_G(x)^2\rangle). \tag{1.1}$$

Here, Φ denotes the primordial curvature perturbations (Bardeen's gauge-invariant potential), $\phi_G(x)$ is a Gaussian random field, and the constant f_{NL} is the parameter describing deviations from Gaussianity. The local model has been much studied for its simplicity — it

contains the first two terms of the most general local form of non-Gaussianity (e.g. [9, 10]). In a recent paper ([11]; hereafter BHK11), we introduced a generalization of this model to one where, in Fourier space, $f_{\mathrm{NL}} = f_{\mathrm{NL}}(k)$ is a function of scale

$$\Phi(k) = \phi_G(k) + f_{\mathrm{NL}}(k) \int \frac{d^3 k'}{(2\pi)^3} \phi_G(k') \phi_G(k - k').\tag{1.2}$$

This is a natural extension of the popular 'local' model[1] $f_{\mathrm{NL}} = \mathrm{const}$, and it is physically well-motivated; it can describe inflationary scenarios with multiple light fields, one of which is responsible for the generation of curvature perturbations [13–15]. The bispectrum in this generalized local model is

$$B_\phi(k_1, k_2, k_3) = 2[f_{\mathrm{NL}}(k_1) P_\phi(k_2) P_\phi(k_3) + \mathrm{perm.}],\tag{1.3}$$

where P_ϕ is the power spectrum of potential fluctuations. This reduces to the familiar expression $B(k_1, k_2, k_3) = 2 f_{\mathrm{NL}}(P_\phi(k_1) P_\phi(k_2) + \mathrm{perm.})$ when f_{NL} is a constant.

To parametrize this model while retaining its full generality, it is convenient to consider a parametrization in piecewise-constant bins in wavenumber:

$$f_{\mathrm{NL}}^i \equiv f_{\mathrm{NL}}(k_i)\tag{1.4}$$

where each f_{NL}^i is the value of $f_{\mathrm{NL}}(k)$ in the i-th wavenumber bin. In BHK11, we used this parametrization to project errors on $f_{\mathrm{NL}}(k)$ from a hypothetical Stage III galaxy survey. As in BHK11, we adopt 20 bins in wavenumber distributed uniformly in $\log(k)$, which is easily sufficient to obtain the best-measured principal components accurately.

In this work, we perform an analysis that is similar in spirit to that in BHK11, but extended in several respects. First of all, we develop formalism and work out forecasts for how well the CMB, in particular Planck [16], can measure $f_{\mathrm{NL}}(k)$. We combine this with the LSS forecasts updated to reflect three specific galaxy surveys. Having done that, we obtain a clearer picture of where we can expect good constraints on non-Gaussianity in k-space. Finally, we project our forecasts to the specific, power-law model in wavenumber, and thus clarify at which wavenumber the CMB, LSS and the combined surveys best determine non-Gaussianity. Therefore, this work complements not only BHK11 and studies that forecasted errors for (occasionally slightly different) models of scale-dependent non-Gaussianity [14, 17, 18], but also many previous forecasts for future constraints on *constant* f_{NL} [18–32].

The structure of this paper is as follows: in section 2, we briefly review the main result from BHK11 — the signature of the generalized local model on large-scale structure through halo bias — and explore the effects of an additional term in the modeling of non-Gaussian bias first pointed out by Desjacques et al. [33]. In section 3, we find the signature of the generalized local model on the CMB bispectrum, with particular emphasis on Planck. Finally, in section 4 we combine the results for a set of joint constraints; we also perform a principal-component analysis, and project constraints on a power-law model of $f_{\mathrm{NL}}(k)$. We conclude in section 5. Details of the computational work can be found in the appendices.

---

[1]This is not the most general scale-dependent model possible, as it is certainly possible to promote f_{NL} to a function of (k_1, k_2, k_3), among other possibilities. Scale-depenent non-gaussianity is also a generic feature of models with modified gravity. One can also introduce scale-dependence to a different model of non-Gaussianity altogether; for example, the Dirac-Born-Infeld braneworld theory typically leads to scale-dependent equilateral f_{NL}, which has been constrained in ref. [12].

2 Generalized local model: signatures in large-scale structure

In this section we first briefly review how the general local model of non-Gaussianity affects the bias of dark matter halos. We then present details of the LSS surveys that we will consider.

2.1 Effect on the bias

For the local non-Gaussian model from eq. (1.1), the dark matter halo bias acquires scale dependence [34]:

$$b(k) = b_0 + \Delta b(k) = b_0 + f_{\rm NL}(b_0 - 1)\delta_c \frac{3\Omega_m H_0^2}{a\, g(a)T(k)c^2 k^2}, \tag{2.1}$$

where b_0 is the usual Gaussian bias (on large scales, where it is constant), $\delta_c \approx 1.686$ is the collapse threshold, a is the scale factor, Ω_m is the matter density relative to the critical density, H_0 is the Hubble constant, k is the wavenumber, $T(k)$ is the transfer function, and $g(a)$ is the growth suppression factor.[2] See also [22, 28, 35–48] who explored the effects of primordial non-Gaussianity on the bias of dark matter halos in great detail.

In BHK11, we worked out the signature of the generalized local model, using the MLB formalism [35, 49, 50], and made forecasts for future galaxy surveys. It is not our intention to fully repeat all of our analysis from that paper, and we just quote essential results. The change in the bias Δb is given, in the generalized local model, by eq. (3.16) from BHK11

$$\frac{\Delta b}{b}(k) = \frac{\delta_c}{D(z)} \frac{2}{8\pi^2\sigma_R^2 \mathcal{M}_R(k)} \int dk_1 k_1^2 \mathcal{M}_R(k_1)P_\phi(k_1)$$
$$\times \int d\mu \mathcal{M}_R(k_2) \left[f_{\rm NL}(k)\frac{P_\phi(k_2)}{P_\phi(k)} + 2f_{\rm NL}(k_2) \right]. \tag{2.2}$$

where $\mathcal{M}_R(k) \equiv [k^2 T(k)\tilde{W}_R(k)]/(H_0^2\Omega_m)$ and $\tilde{W}_R(k)$ is the Fourier transform of the top-hat filter with radius R. The derivatives with respect to piecewise constant parameters $f_{\rm NL}^i$ are straightforward and given by eq. (3.19) of our previous paper.

However eq. (2.2) is not entirely correct in describing the scale-dependent bias from a general NG model. Desjacques et al. ([33]; see also [45]) pointed out that the expression (2.1) is only correct in the high-peak, small-k limit. An additional term is required for the exact expression:

$$\Delta b(k) = \frac{2F(k)}{M_R(k)D(z)} \left[(b_0 - 1)\delta_c + \frac{d\ln F(k)}{d\ln\sigma_R} \right] \tag{2.3}$$

where

$$F(k) = \frac{1}{8\pi^2\sigma_R^2} \int dk_1 k_1^2 \mathcal{M}_R(k_1)P_\phi(k_1) \int_{-1}^{1} d\mu \mathcal{M}_R(k_2) \left[f_{\rm NL}(k)\frac{P_\phi(k_2)}{P_\phi(k)} + 2f_{\rm NL}(k_2) \right]. \tag{2.4}$$

The new term (second term in square parentheses in eq. (2.3)) vanishes when the fiducial model for non-Gaussianity is $f_{\rm NL}(k) = {\rm const}$, but it becomes relevant for truly scale-dependent models, including the piecewise-constant parametrization of $f_{\rm NL}(k)$ from equation (1.4). Because we are expanding (taking Fisher derivatives) around the constant value of $f_{\rm NL}(k)$ (30 or zero), we find very small though nonzero effect of this new term describing halo bias. See appendix C for details.

---

[2] The usual linear growth $D(a)$, normalized to be equal to a in the matter-dominated epoch, is related to the suppression factor $g(a)$ via $D(a) = ag(a)/g(1)$, where $g(a)$ is normalized to be equal to unity deep in the matter-dominated epoch.

2.2 Fisher matrix analysis: assumptions and survey specifications

We are interested in making forecasts for constraints on non-Gaussianity from future galaxy surveys, and for this we employ the standard Fisher matrix formalism.

For measurements of the power spectrum of dark matter halos, the Fisher matrix F is [51]

$$F_{ij}^{\mathrm{LSS}} = \sum_m V_m \int_{k_{\min}}^{k_{\max}} \frac{\partial P_h(k, z_m)}{\partial p_i} \frac{\partial P_h(k, z_m)}{\partial p_j} \frac{1}{\left[P_h(k, z_m) + \frac{1}{n} \right]^2} \frac{k^2 dk}{(2\pi)^2}, \qquad (2.5)$$

where V_m is the comoving volume of the m-th redshift bin, each redshift bin is centered on z_m, and we have summed over all redshift bins. We adopt[3] $k_{\min} = 10^{-4} h^{-1} \mathrm{Mpc}$, and we choose $k_{\max}$ as a function of z so that $\sigma(\pi/(2k_{\max}), z) = 0.5$ [52], which leads to $k_{\max}(z = 0) \approx 0.1 h \mathrm{Mpc}^{-1}$. P_h is the dark matter halo power spectrum, related to the true dark matter power spectrum P through

$$P_h(k) = b(k)^2 P(k), \qquad (2.6)$$

where each quantity implicitly also depends on redshift. Finally, p_i are the parameters of interest; in our case, these are the f_{NL}^i, cosmological parameters, and the bias-related nuisance parameters listed below in (2.7). The minimal error in the i-th cosmological parameter is, by the Cramér-Rao inequality, $\sigma(p_i) \simeq \sqrt{(F^{-1})_{ii}}$.

All of the results cited in this section, as well as LSS survey projections elsewhere in this paper, assume the following survey properties, modeled on BigBOSS [53], unless explicitly stated otherwise. We adopt the fiducial value $f_{\mathrm{NL}} = 30$, chosen to roughly correspond to the maximum-likelihood value favored by current CMB data [54]. The fiducial cosmological model is the standard ΛCDM model with Hubble's constant H_0; physical dark matter and baryon densities $\Omega_{\mathrm{cdm}}h^2$ and $\Omega_{\mathrm{b}}h^2$; equation of state of dark energy w; the log of the scalar amplitude of the matter power spectrum, $\log A_s$; and the spectral index of the matter power spectrum, n_s. Fiducial values of these parameters correspond to their best-fit WMAP7 values [54]. We also added the forecasted cosmological parameter constraints from the CMB experiment Planck by adding its Fisher matrix as a prior (W. Hu, private communication). Note that the CMB prior does *not* include CMB constraints on non-Gaussianity, so that we are not double-counting the latter constraints. Next, we include twenty piecewise-constant non-Gaussianity parameters $f_{\mathrm{NL}}(k_i) \equiv f_{\mathrm{NL}}^i$ with $i = 0, 1, \ldots, 19$. Finally, we include a Gaussian bias parameter in our Fisher matrix, $b_0(z)$, for each of the 44 redshift bins over the range $0.1 < z < 4.5$ (which is discussed further below). The full list of parameters that we have in the BigBOSS Fisher matrix is

$$\{p_i\} = \{H_0, \Omega_{\mathrm{cdm}}h^2, \Omega_{\mathrm{b}}h^2, w, \log A_s, n_s, b_0^1, \ldots, b_0^{44}, f_{\mathrm{NL}}^0, \ldots, f_{\mathrm{NL}}^{19}\} \qquad (2.7)$$

BigBOSS will utilize three different tracers: LRGs, ELGs, and QSOs. The fiducial values for $b_0(z = 0)$ are different for each of the three tracers, as are the number densities. To account for this, we calculated the Fisher matrix for each tracer, then added all three together for

---

[3] We found that the constraints are insensitive to the precise value of $k_{\min}$ for the fiducial $f_{\mathrm{NL}}(k) = 30$ (or any sufficiently nonzero value), since the most constraining scales are intermediate between $k_{\min}$ and $k_{\max}$, reflecting the competition between larger noise and larger signal as one goes to lower k. However, for the fiducial value $f_{\mathrm{NL}}(k) = 0$ the constraints indeed come from the largest available scales, and in that case we adopt $k_{\min} = V_{\mathrm{survey}}^{-1/3}$.

the final BigBOSS Fisher matrix. The fiducial values for $b_0(z = 0)$ were 1.7 for the LRGs, 0.84 for the ELGs, and 1.2 for the QSOs [55]. In each case, we assume the simple scaling of b_0 with redshift, $b_0(z) = b_0(z = 0)/D(z)$.

In order to simplify the analysis, and in light of the uncertainties of the distribution of *observed* LSS tracers' masses, we assume a fixed halo mass of $10^{13} M_\odot/h$. Since we marginalize over b_0 in each redshift bin, we effectively delete much information about the mass of the tracers. Essentially, we utilize information about the redshift- and wavenumber-dependence of bias, but avoid — at least for now — using information about the masses, since accurate masses of LSS tracers are typically very difficult to obtain, except for galaxy clusters.

We assume that BigBOSS will cover 14,000 square degrees. The redshift ranges for the LRGs, ELGs and QSOs are $z_{\max}^{\rm LRG} = 1.2$, $z_{\max}^{\rm ELG} = 1.8$ and $z_{\max}^{\rm QSO} = 4.5$; the forecasted number density in each redshift bin of course widely vary, and in particular the QSOs have much lower typical number densities per redshift bin than the other tracers [55]. We split the survey into the aforementioned 44 redshift bins out to $z_{\max} = 4.5$; the total volume of the survey is therefore $V_{\rm tot} = 230 \, (h^{-1} {\rm Gpc})^3$. The errors in the cosmological parameters vary, in the cosmic variance limit, as $V_{\rm tot}^{-1/2}$.

In addition to presenting our results with the fiducial BigBOSS survey (14,000 sq. deg., $z_{\max} = 4.5$), we also forecast constraints for the Dark Energy Survey (DES [56]), which will cover 5,000 sq. deg. with $z_{\max} = 1.0$, split into 5 redshift bins. For simplicity's sake, we assume that this survey will only see one tracer, with a fiducial Gaussian bias $b_0(z = 0) = 2.0$ and a number density $n = 2 \times 10^{-4} \, (h \, {\rm Mpc}^{-1})^3$ (independent of redshift). Note that the actual redshift distribution and number density of the DES tracers will depend on the *spectroscopic followup* to the main survey and the objects that it targets, details of which are somewhat uncertain at this time and hence our approximate assumptions. The rest of the Fisher matrix formalism for this survey (cosmological parameters, etc.) is the same as what we used for the BigBOSS Fisher matrix.

2.3 The effect of the fiducial value on constraints

Looking back at Equation (2.5), we see that the fiducial $f_{\rm NL}$ enters through the bias, by way of P_h. Assuming $P_h(k) \gg 1/n$ (a reasonable assumption at large angular scales where non-Gaussianity constraints largely come from and where shot noise is negligible), we find that the Fisher matrix element corresponding to $f_{\rm NL} = {\rm const}$ is

$$F^{\rm LSS} \propto \int \left(\frac{\partial b(k)}{\partial f_{\rm NL}} \right)^2 b^{-2}(k) dk = \int \left(\frac{\Delta b(k)}{f_{\rm NL} \, (b_0 + \Delta b(k))} \right)^2 dk \qquad (2.8)$$

Thus, the expression on the right-hand side will, in general, be dependent on the choice of fiducial $f_{\rm NL}$. Since $|\Delta b(k)|$ blows up at small k, in that regime we have:

$$\left(\frac{\Delta b(k)}{f_{\rm NL} \, (b_0 + \Delta b(k))} \right)^2 \approx \frac{1}{f_{\rm NL}^2} \qquad (2.9)$$

At large k, $\Delta b(k)$ goes to 0, taking the entire expression with it. Thus, the integral is dominated by the contribution at low k, meaning we should expect a maximal Fisher matrix element around a fiducial $f_{\rm NL} = 0$. And indeed, that is what we see in figure 1: the projected constraints on $f_{\rm NL}$ from a given sky survey depend strongly on the fiducial value chosen, with the tightest constraints at $f_{\rm NL} = 0$.

We note that, as shown in the following section, the Fisher matrix is independent of the fiducial $f_{\rm NL}$ value for the CMB constraints for our piecewise-constant parameterization.
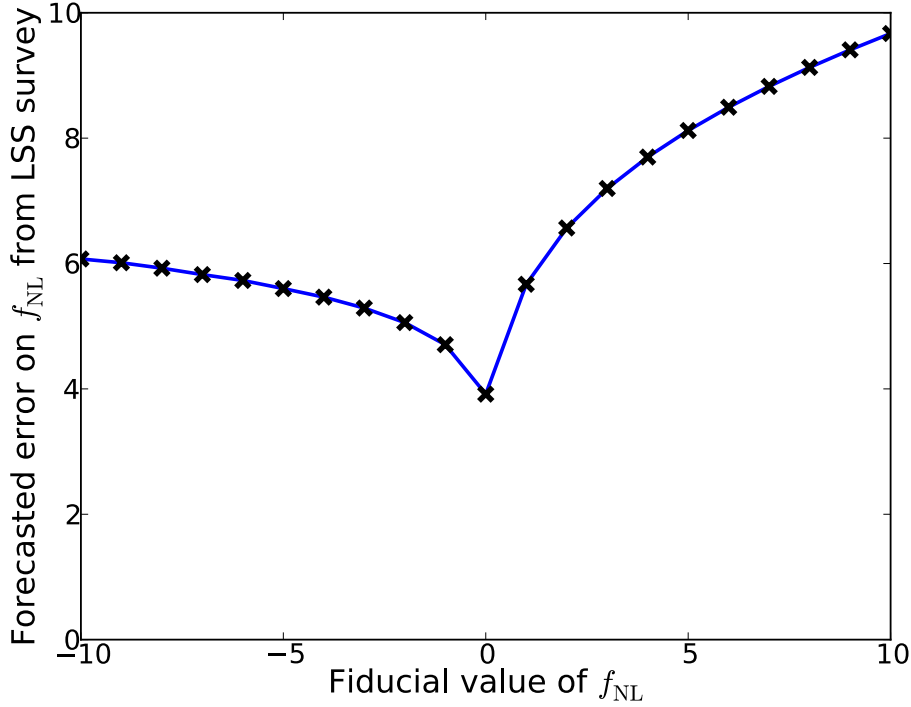
Figure 1. A more detailed look at how the choice of fiducial $f_{\rm NL}$ affects the projected constraints on *constant* $f_{\rm NL}$ from a future galaxy survey. See text for analytic explanation for why results are the best at fiducial value of $f_{\rm NL} = 0$.

3 Generalized local model: signatures in the CMB

Traditionally, the best constraints on non-Gaussianity have come from the CMB. This is done almost exclusively through estimators involving the N-point correlation functions for $N > 2$ and their Fourier transforms, the polyspectra. Most emphasis has been on the $N = 3$ case, or the bispectrum of temperature fluctuations in the CMB, if only because of its relative computational simplicity. The well-known general expression for the CMB bispectrum, re-derived in appendix A, is

$$B^{pqr}_{\ell_1\ell_2\ell_3} = \left(\frac{2}{\pi}\right)^3 \sqrt{\frac{(2\ell_1+1)(2\ell_2+1)(2\ell_3+1)}{4\pi}} \begin{pmatrix} \ell_1 & \ell_2 & \ell_3 \\ 0 & 0 & 0 \end{pmatrix} \int k_1^2 dk_1\, k_2^2 dk_2\, k_3^2 dk_3$$
$$\times B_\Phi(k_1,k_2,k_3) t^p_{\ell_1}(k_1) t^q_{\ell_2}(k_2) t^r_{\ell_3}(k_3) \int_0^\infty r^2 dr\, j_{\ell_1}(k_1 r) j_{\ell_2}(k_2 r) j_{\ell_3}(k_3 r) \quad (3.1)$$

where the expression in angular parentheses is the Wigner-3j symbol, B_Φ is the curvature bispectrum, and t_ℓ are the radiation transfer functions.

In principle, we can use this to find the Fisher matrix F_{ij} for the CMB bispectrum and thus forecast how well the CMB bispectrum can determine the cosmological

parameters: [5, 8, 57, 58]

$$F_{ij}^{\mathrm{CMB}} = f_{\mathrm{sky}} \sum_{lmn,pqr} \sum_{2 \leq \ell_1 \leq \ell_2 \leq \ell_3} \frac{1}{\Delta_{\ell_1 \ell_2 \ell_3}} \frac{\partial B_{\ell_1 \ell_2 \ell_3}^{lmn}}{\partial p_i} (\mathbf{C}_{\ell_1 \ell_2 \ell_3}^{-1})_{lmn,pqr} \frac{\partial B_{\ell_1 \ell_2 \ell_3}^{pqr}}{\partial p_j}. \tag{3.2}$$

Here, $\mathbf{C}$ is the covariance of the bispectra and $p_{i,j}$ are the parameters of interest. $\Delta_{\ell_1 \ell_2 \ell_3}$ is a combinatoric term — equal to 6 when $\ell_1 = \ell_2 = \ell_3$, 1 when $\ell_1 \neq \ell_2 \neq \ell_3$, and 2 otherwise [58]. The indices i, j, k and p, q, r run independently over all eight possible ordered triplets of temperature and polarization fields (TTT, TTE...EEE). The details of calculating $B_{\ell_1 \ell_2 \ell_3}^{pqr}$ and its derivatives are in appendix A, while the details of calculating the bispectrum covariance $\mathbf{C}$ are in appendix B.

Equation (3.1) is a totally general result for the bispectrum of the CMB in terms of the Bardeen curvature bispectrum; we have not picked any model of non-Gaussianity. But (3.1) is not useful without picking a form for $B_\Phi(k_1, k_2, k_3)$. For the constant f_{NL} case, we have the following Bardeen curvature bispectrum:

$$B_\Phi(k_1, k_2, k_3) = 2\Delta_\phi^2 f_{\mathrm{NL}} \left(\frac{1}{k_1^{3-(n_s-1)} k_2^{3-(n_s-1)}} + \mathrm{perm.} \right) \tag{3.3}$$

where Δ_ϕ is the amplitude of the curvature power spectrum. Using eqs. (3.2), (B.4), and (A.24), we have the following expression for the CMB bispectrum Fisher information in the constant f_{NL} case:

$$
\begin{aligned}
F_{f_{\mathrm{NL}}}^{\mathrm{CMB}} = {}& 4\Delta_\phi^4 \sum_{lmn,pqr} \sum_{2 \leq \ell_1 \leq \ell_2 \leq \ell_3} \frac{1}{\Delta_{\ell_1 \ell_2 \ell_3}} \frac{(2\ell_1+1)(2\ell_2+1)(2\ell_3+1)}{4\pi} \begin{pmatrix} \ell_1 & \ell_2 & \ell_3 \\ 0 & 0 & 0 \end{pmatrix}^2 \frac{1}{\Delta_{\ell_1 \ell_2 \ell_3}} \\
& \times (C_{\ell_1}^{-1})_{lp}(C_{\ell_2}^{-1})_{mq}(C_{\ell_3}^{-1})_{nr} \left[\int_0^\infty r^2 dr \left(\alpha_{\ell_1}^l(r)\beta_{\ell_2}^m(r)\beta_{\ell_3}^n(r) + \mathrm{perm.} \right) \right] \\
& \times \left[\int_0^\infty r^2 dr \left(\alpha_{\ell_1}^p(r)\beta_{\ell_2}^q(r)\beta_{\ell_3}^r(r) + \mathrm{perm.} \right) \right]
\end{aligned} \tag{3.4}
$$

where α_ℓ and β_ℓ are defined in equations (A.21) and (A.22).

For the *scale-dependent* $f_{\mathrm{NL}}(k)$ case from our generalized ansatz, things are somewhat more complicated. The Bardeen curvature bispectrum is:

$$B_\Phi(k_1, k_2, k_3) = 2\Delta_\phi^2 \left(\frac{f_{\mathrm{NL}}(k_3)}{k_1^{3-(n_s-1)} k_2^{3-(n_s-1)}} + \mathrm{perm.} \right). \tag{3.5}$$

Using the piecewise-constant parametrization of $f_{\mathrm{NL}}(k)$, eqs. (3.2), (B.4), and (A.25) yield the following expression for the Fisher matrix of all the f_{NL}^i in the scale-dependent case, similar to eq. (3.4):

$$
\begin{aligned}
F_{ij}^{\mathrm{CMB}} = {}& 4\Delta_\phi^4 \sum_{lmn,pqr} \sum_{2 \leq \ell_1 \leq \ell_2 \leq \ell_3}^{\ell_{\mathrm{max}}} \frac{1}{\Delta_{\ell_1 \ell_2 \ell_3}} \frac{(2\ell_1+1)(2\ell_2+1)(2\ell_3+1)}{4\pi} \begin{pmatrix} \ell_1 & \ell_2 & \ell_3 \\ 0 & 0 & 0 \end{pmatrix}^2 \\
& \times \frac{1}{\Delta_{\ell_1 \ell_2 \ell_3}} (C_{\ell_1}^{-1})_{ip}(C_{\ell_2}^{-1})_{jq}(C_{\ell_3}^{-1})_{kr} \left[\int_0^\infty r^2 dr \left(\alpha_{\ell_1}^{l,i}(r)\beta_{\ell_2}^m(r)\beta_{\ell_3}^n(r) + \mathrm{perm.} \right) \right] \\
& \times \left[\int_0^\infty r^2 dr \left(\alpha_{\ell_1}^{p,j}(r)\beta_{\ell_2}^q(r)\beta_{\ell_3}^r(r) + \mathrm{perm.} \right) \right].
\end{aligned} \tag{3.6}
$$

Despite appearances, this is a relatively straightforward calculation to perform, and it takes roughly an hour (on four processors) for twenty f_{NL}^i parameters with $\ell_{\max} \approx 2000$.

We did not include other cosmological parameters in the CMB bispectrum Fisher matrix, since the bispectrum does not constrain them terribly well, while on the other hand the CMB *power* spectrum places very good constraints on the other cosmological parameters. In other words, non-Gaussianity estimates obtained using the CMB bispectrum would not be significantly affected by marginalizing over the other cosmological parameters within their allowed ranges, as explicitly shown by ref. [59]. Therefore, it is a fair (and certainly very helpful) approximation to think the CMB power spectrum and the bispectrum complementing each other by constraining the standard cosmological parameters, and the non-Gaussian parameters, respectively and separately. This has indeed been the approach in the literature (e.g. [8, 57]).

4 Results and joint constraints

4.1 Forecasted constraints on the f_{NL}^i

Figure 2 shows the (unmarginalized) constraints on the piecewise constant parameters f_{NL}^i in the generalized local model from BigBOSS and Planck individually, as well as combined. Note that the two types of surveys have comparable constraints at the pivot wavenumber, but the pivot is at a larger wavenumber for BigBOSS. Away from the pivot, the Planck constraints are expected to be better than those from BigBOSS, but both rapidly deteriorate away from their respective pivots. Finally, the combined constraints are significantly helped by the lever arm in wavenumber when the two probes are combined, and this leads to better constraints across a wider range of scales. We will make these statements more quantitative below when we study the specific case where $f_{\mathrm{NL}}(k)$ is a pure power law in k.

The horizontal green curves in all panels in figure 2 show the accuracy in the constant f_{NL}, projected down from the principal components f_{NL}^i as described in BHK11. The accuracy achieved in f_{NL} is 4.4 for Planck, 2.6 for BigBOSS, and 2.2 for the combined case. Recall also that our Fisher matrices for Planck — but not for BigBOSS — assume all cosmological parameters other than the f_{NL}^i are fixed (known).

4.2 Principal component analysis

Following BHK11, we now represent a general function $f_{\mathrm{NL}}(k)$ in terms of principal components (PCs). In this approach, the *data* determine which particular modes of $f_{\mathrm{NL}}(k)$ are best or worst measured. The PCs also constitute a useful form of data compression, so that one can keep only a few of the best-measured modes to make inferences about the function $f_{\mathrm{NL}}(k)$. The PCs are weights in wavenumber with amplitudes that are uncorrelated by construction, and they are ordered from the best-measured ($i = 0$) to the worst-measured ($i = 19$) for the assumed fiducial survey. We follow the construction of the PCs following the formalism outlined in appendix B of BHK11. We assume a total of 20 principal components distributed uniformly in $\log(10^{-4}\, h\,\mathrm{Mpc}^{-1}) \leq \log(k) \leq \log(1\, h\,\mathrm{Mpc}^{-1})$, which is easily sufficient to make model-independent statements about $f_{\mathrm{NL}}(k)$.

Figure 3 shows the forecasted PCs of LSS and Planck separately and combined. Heuristically, the lowest principal component (PC0) serves to see how well we can find the deviation of $f_{\mathrm{NL}}(k)$ at its pivot (i.e. best-determined wavenumber) from the fiducial value. The higher PCs (PC1, PC2, etc) serve to probe the k-dependence of f_{NL}.

Figure 4 shows the 1-σ errors on the PCs for BigBOSS, Planck, and the two combined. Note that the BigBOSS errors are slightly smaller than those from Planck (the DES errors, not shown here, are bigger than Planck's). Combining BigBOSS and Planck sharply decreases
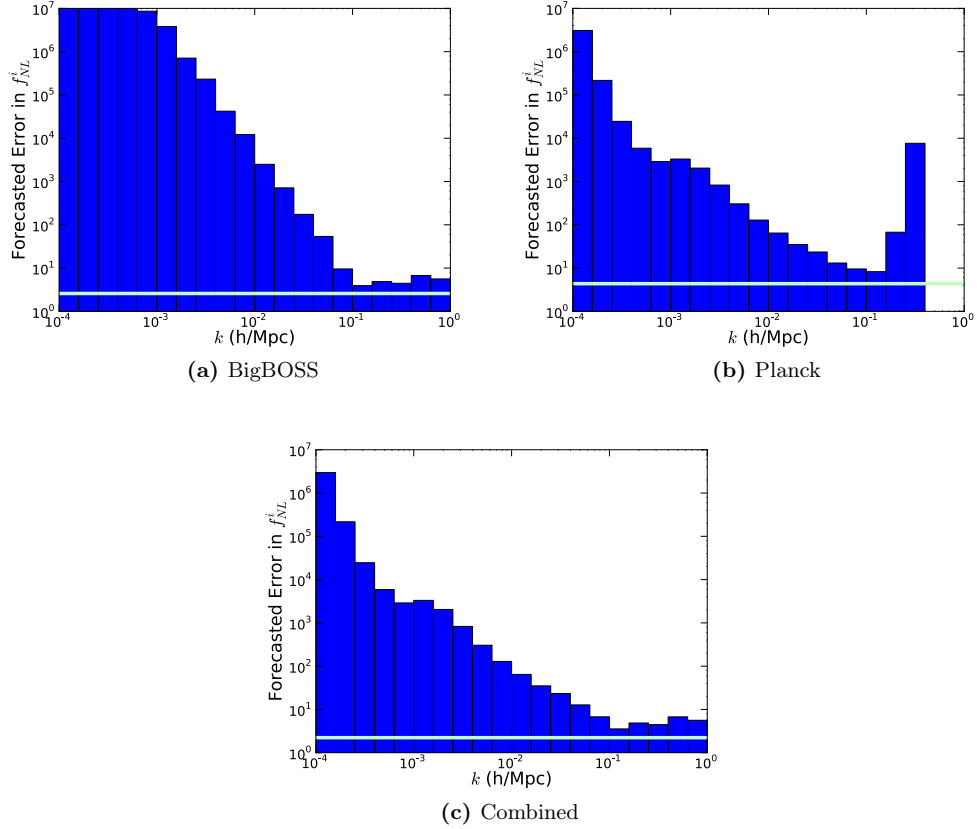
Figure 2. Constraints on the piecewise constant parameters $f_{\rm NL}^i$ in the generalized local model with the LSS (top left), CMB (top right), and LSS+CMB (bottom). The fiducial model around which we perturbed was a level of non-Gaussianity consistent with the preferred value from WMAP, $f_{\rm NL}^i = 30$. All constraints are unmarginalized, in order to more clearly show the wavenumber-dependent sensitivity of the probes to primordial non-Gaussianity. The LSS constraints come from the power spectrum of galaxies, while the CMB constraints come from the bispectrum of temperature fluctuations. See text for details. For reference, the green line is the constraint found for a constant $f_{\rm NL}$ using the same assumptions. There are bins "missing" on the rightmost end of the Planck plot; those bins correspond to k-values too large to be probed when $\ell_{\rm max} = 2000$, as it is here.

the errors. Note too that for fiducial $f_{\rm NL}(k) = 0$, BigBOSS only constraints $f_{\rm NL}(k)$ at the pivot point well (as shown below in figure 7), and hence the error in the best-determined principal component is noticeably smaller than errors in the other PCs.

The relative strength of the LSS and CMB constraints at their respective pivot points strongly depend on two factors: volume of the LSS survey and, to a slightly lesser extent, fiducial (i.e. true) value of $f_{\rm NL}(k)$ (the CMB is not as sensitive to the fiducial value of $f_{\rm NL}(k)$). For example, for $f_{\rm NL}(k) = 30$ and DES we find that Planck constraints at the CMB pivot are stronger, while assuming BigBOSS survey we find that the LSS is slightly stronger at its own pivot. In addition, the CMB typically constrains $f_{\rm NL}(k)$ over a wider range of scales than the LSS.
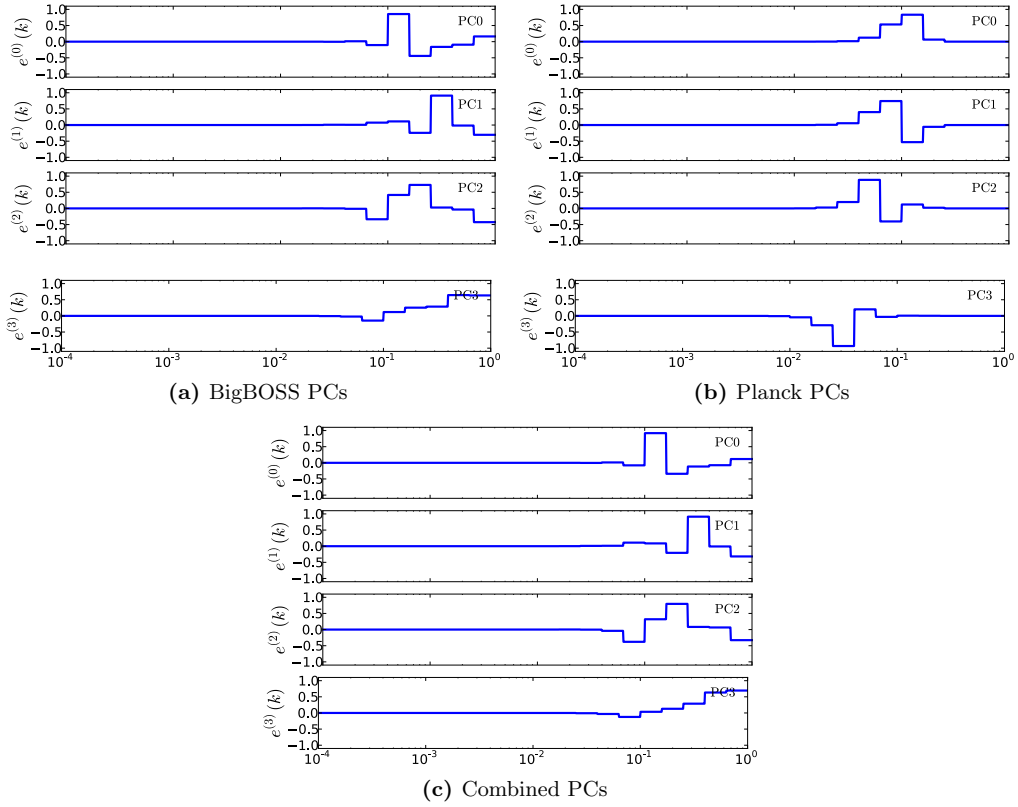
(a) BigBOSS PCs

(b) Planck PCs

(c) Combined PCs

Figure 3. The first four forecasted principal components of $f_{\rm NL}(k)$ from BigBOSS, Planck, and BigBOSS+Planck, assuming the fiducial model $f_{\rm NL}(k) = 30$. The PCs eigenvectors $e^{(j)}(k)$ are ordered from the best-measured one ($j = 0$) to the worst-measured one ($j = 19$; not shown here) for the assumed fiducial survey.
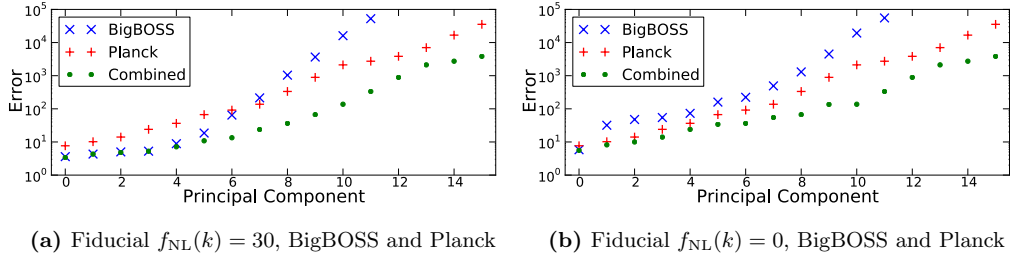

(a) Fiducial $f_{\rm NL}(k) = 30$, BigBOSS and Planck

(b) Fiducial $f_{\rm NL}(k) = 0$, BigBOSS and Planck

Figure 4. RMS error on each principal component for BigBOSS, Planck, and the two combined. Note that the BigBOSS errors are slightly smaller than those from Planck; in all cases combining the CMB and LSS decreases errors. Note too that for fiducial $f_{\rm NL}(k) = 0$ (right panel) BigBOSS only constraints $f_{\rm NL}(k)$ at the pivot point well (see figure 7), and hence the error in the best-determined principal component is noticeably smaller than errors in the other PCs.

4.3 Projecting constraints on the power-law model of $f_{\rm NL}(k)$

Once the Fisher matrix F has been obtained for the set of parameters $f_{\rm NL}^i$, it is quite simple to find the best possible constraints on the $f_{\rm NL}^i$ that could be obtained from a future galaxy redshift survey. By projecting this Fisher matrix into another basis, it is also possible to find the constraints on any arbitrary $f_{\rm NL}(k)$ without calculating a new Fisher matrix from scratch.

Here we will study the popular simple form of non-Gaussianity analogous to the conventional parameterization of the power spectrum [17, 60–64]

$$f_{\rm NL}(k) = f_{\rm NL}^* \left(\frac{k}{k_*} \right)^{n_{f_{\rm NL}}} , \tag{4.1}$$

where k_* is an arbitrary fixed parameter, leaving $f_{\rm NL}^*$ and $n_{f_{\rm NL}}$ as the parameters of interest in this model. The partial derivatives of our basis of $f_{\rm NL}^i$ with respect to these parameters are:

$$\frac{\partial f_{\rm NL}^i}{\partial f_{\rm NL}^*} = \left(\frac{k_i}{k_*} \right)^{n_{f_{\rm NL}}} ; \tag{4.2}$$

$$\frac{\partial f_{\rm NL}^i}{\partial n_{f_{\rm NL}}} = f_{\rm NL}^* \left(\frac{k_i}{k_*} \right)^{n_{f_{\rm NL}}} \log \left(\frac{k_i}{k_*} \right) , \tag{4.3}$$

where k_i is the k at the center of the ith k-bin. Starting in a basis of 20 $f_{\rm NL}^i$ evenly spaced in log k, we project down to a basis of $f_{\rm NL}^*$ and $n_{f_{\rm NL}}$ in order to forecast constraints on the two new parameters. [Note that k_* is an arbitrarily chosen parameter which differs in general from the true pivot $k_{\rm piv}$ where constraints on $f_{\rm NL}(k)$ are the best. The choice of k_* affects neither the constraints on $f_{\rm NL}(k)$ nor the value of $k_{\rm piv}$.]

We can use the constraints on $f_{\rm NL}^*$ and $n_{f_{\rm NL}}$ to find constraints on $f_{\rm NL}(k)$ as a whole, through the usual methods of error propagation:

$$\sigma(f_{\rm NL}(k)) = \sqrt{ \left(\frac{\partial f_{\rm NL}}{\partial f_{\rm NL}^*} \sigma(f_{\rm NL}^*) \right)^2 + \left(\frac{\partial f_{\rm NL}}{\partial n_{f_{\rm NL}}} \sigma(n_{f_{\rm NL}}) \right)^2 + 2 \frac{\partial f_{\rm NL}}{\partial f_{\rm NL}^*} \frac{\partial f_{\rm NL}}{\partial n_{f_{\rm NL}}} C_{f_{\rm NL}^*, n_{f_{\rm NL}}} } , \tag{4.4}$$

where $C_{f_{\rm NL}^*, n_{f_{\rm NL}}}$ is the covariance between $f_{\rm NL}^*$ and $n_{f_{\rm NL}}$, and $\sigma(f_{\rm NL}^*)^2$ and $\sigma(n_{f_{\rm NL}})^2$ are their respective variances. Using this relation, and given some fiducial model of $f_{\rm NL}(k)$, we can plot the forecasted constraints on $f_{\rm NL}(k)$ as a function of k. This is what we have done in figure 5 for the Planck bispectrum, DES power spectrum, and the two combined (along with priors on cosmological parameters from the Planck power spectrum).

Figure 6 is analogous to figure 5, but shows BigBOSS and Planck constraints (rather than DES and Planck) for the fiducial value of $f_{\rm NL}(k) = 30$. Note that the forecasted BigBOSS constraints are, very roughly, comparable to those from Planck (see also table 1), but are also very complementary to Planck since their best constraints are at a higher k. Our forecasted constraints on the accuracy of measuring the running with BigBOSS are in good agreement with forecasts for the Euclid survey in ref. [18].

We also introduce the figure of Merit (FoM$^{\rm (NG)}$) of non-Gaussianity. We defined it analogously to the figure of Merit for dark energy ([65]; see also [66]) as

$$\text{FoM}^{\rm (NG)} \equiv (\det F_{2\times 2})^{1/2} \approx \frac{6.17\pi}{A_{95}} \tag{4.5}$$

where $F_{2\times 2}$ is the Fisher matrix projected down to the 2×2 space of $f_{\rm NL}^*$ and $n_{f_{\rm NL}}$, and A_{95} is the area of the 95.4% confidence level ellipse in this space. Constraints on the FoM$^{\rm (NG)}$ are
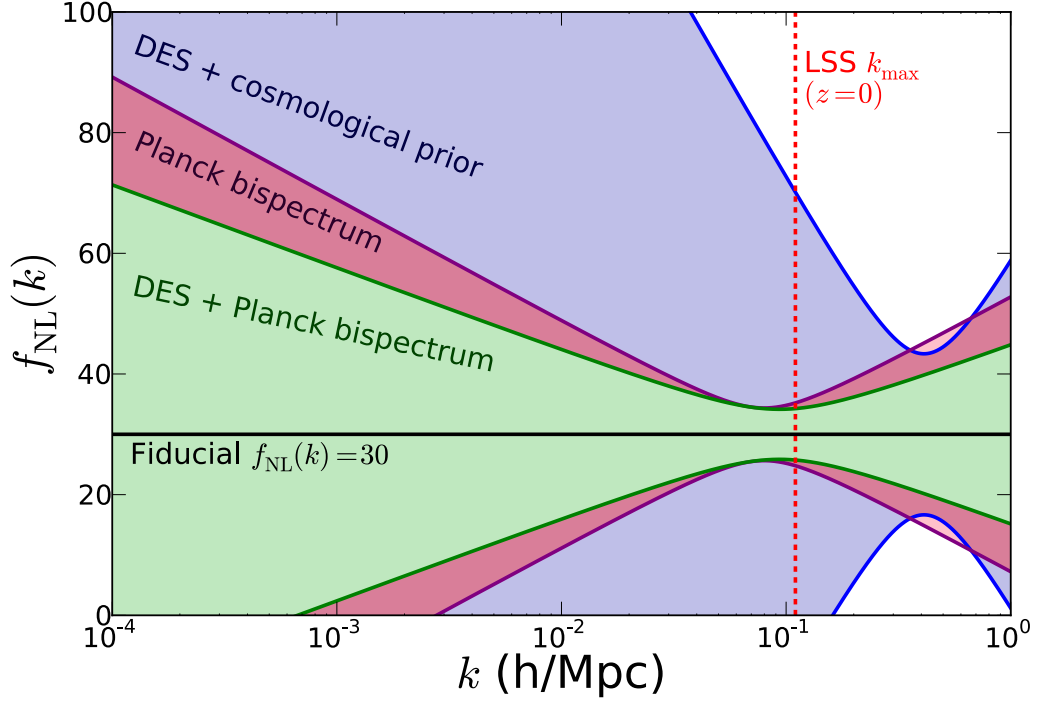
Figure 5. Forecasted constraints on $f_{\mathrm{NL}}(k)$ from several different data sets, assuming the power-law model of scale-dependent non-Gaussianity: $f_{\mathrm{NL}}(k) = f_{\mathrm{NL}}^*(k/k_{\mathrm{piv}})^{n_{f_{\mathrm{NL}}}}$, projecting down from the piecewise-constant f_{NL}^i basis. The red dashed line is the maximum k for which information was kept in the LSS Fisher matrix at $z = 0$. The LSS survey used for this forecast is based on DES.

Projected errors $\sigma(f_{\mathrm{NL}}^*)$ and $\sigma(n_{f_{\mathrm{NL}}})$, and the corresponding pivots				
Variable	BigBOSS	BigBOSS+Planck C_ℓs	Planck bispec	**BigBOSS+all Planck**
$\sigma(f_{\mathrm{NL}}^*)$	3.0	2.6	4.4	2.2
$\sigma(n_{f_{\mathrm{NL}}})$	0.12	0.11	0.29	0.078
FoM$^{(\mathrm{NG})}$	2.7	3.4	0.78	5.8
k_{piv}	0.33	0.35	0.080	0.24

Table 1. Forecasted constraints on f_{NL}^* and $n_{f_{\mathrm{NL}}}$ from BigBOSS, Planck, and combined data sets for two fiducial values of $f_{\mathrm{NL}}(k)$. Each column's numbers are for the pivot in that column; thus the errors in the two parameters are uncorrelated in each column. See text for survey specifications.

presented in table 1, and show that combining of BigBOSS and Planck improves constraints by a factor of between two and five relative to these experiments alone. What is particularly encouraging is that future constraints will improve the recently obtained current constraints on the running of non-Gaussianity [67] by more than an order of magnitude.
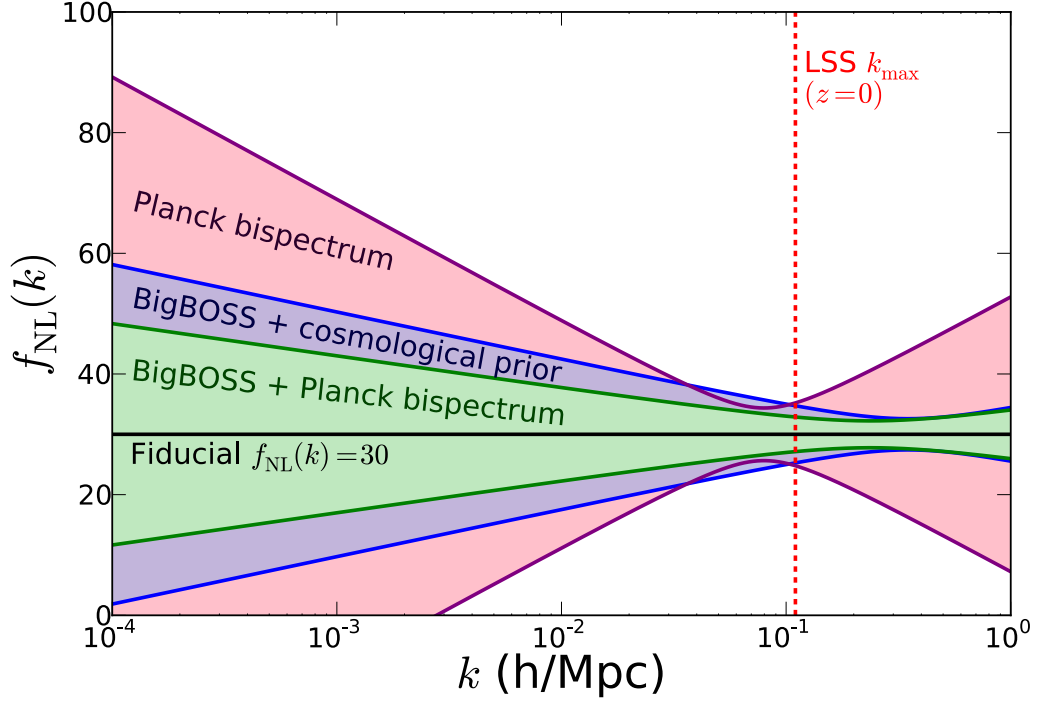
Figure 6. The same as figure 5, but with survey parameters for large-scale structure based on BigBOSS.

Projected errors ($\sigma_{f^*_{\mathrm{NL}}}$, $\sigma_{n_{f_{\mathrm{NL}}}}$) for different fiducial $f_{\mathrm{NL}}(k)$			
	DES	BigBOSS	Planck
Fiducial $f_{\mathrm{NL}}(k) = 30$	(13, 1.0)	(2.6, 0.11)	(4.4, 0.29)
Fiducial $f_{\mathrm{NL}}(k) = 0$	(13, ∞)	(2.5, ∞)	(4.4, ∞)

Table 2. Forecasted constraints $\sigma_{f^*_{\mathrm{NL}}}$ from different LSS surveys, assuming different fiducial models. Forecasted constraints from Planck are also shown for comparison. (All values of $n_{f_{\mathrm{NL}}}$ are equally likely in the second fiducial model, where $f^*_{\mathrm{NL}} = 0$.)

The constraints on $f_{\mathrm{NL}}(k)$ from a large-scale structure survey are quite sensitive to the survey parameters. Unlike the constraints on $f_{\mathrm{NL}}(k)$ from the CMB bispectrum, the forecasted constraints from LSS are also sensitive to the choice made for the fiducial model of $f_{\mathrm{NL}}(k)$, as shown in section 2.3. Forecasted constraints on f^*_{NL} and $n_{f_{\mathrm{NL}}}$ for the DES and BigBOSS surveys, with two different fiducial models, are compared to forecasted constraints from Planck in table 2 (note that *all* values of $n_{f_{\mathrm{NL}}}$ are equally likely for the fiducial model where $f^*_{\mathrm{NL}} = 0$, and hence an infinite error on $n_{f_{\mathrm{NL}}}$). The scale at which the LSS gives the best constraint (the 'sweet spot') turns out to be slightly smaller than the maximum wavenumber assumed to be used by the survey, k_{max}. This is because the halo-bias integration over all the
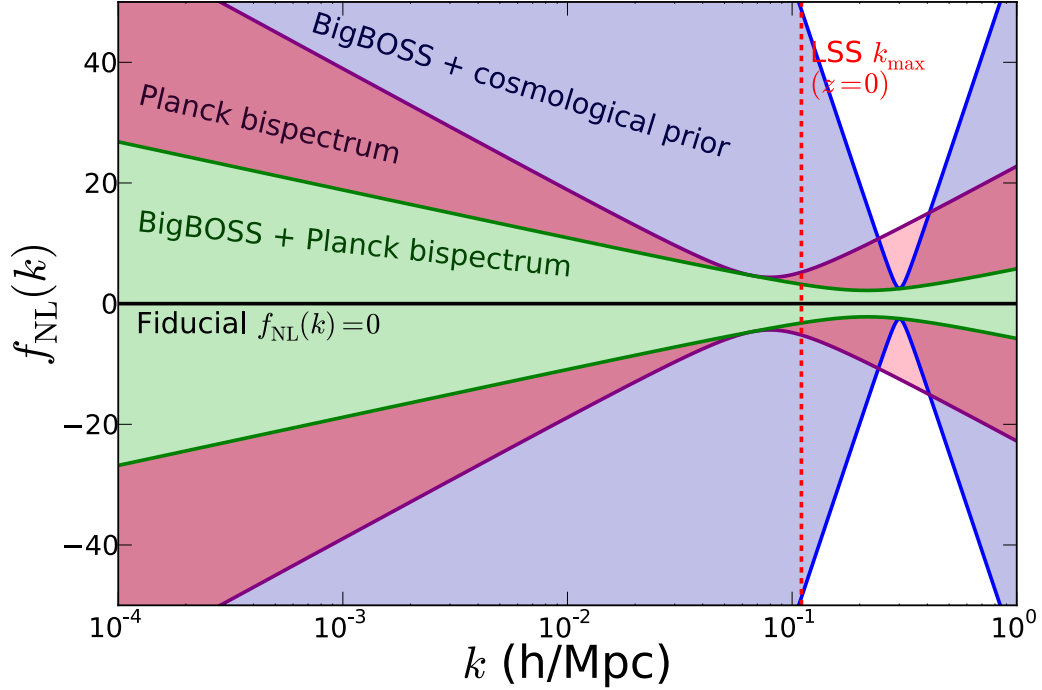
Figure 7. The same as figure 6, but with a fiducial model $f_{\rm NL}(k) = 0$. In the limit $f_{\rm NL}^* \to 0$ there is no information on the running of non-Gaussianity $n_{f_{\rm NL}}$, and hence the LSS/BigBOSS constraints are sharply peaked and essentially constrain $f_{\rm NL}(k)$ at only one wavenumber.

possible momentum space configurations in eq. (2.2) has dominant contributions from small scales,[4] as we noted previously in [11]. Figure 7 shows the same case as figure 6, except for the fiducial value of $f_{\rm NL}(k) = 0$. Because $n_{f_{\rm NL}}$ is arbitrary for this fiducial value, constraints on $f_{\rm NL}(k)$ are only good at a single, pivot wavenumber; this can also be seen by inspection of eqs. (4.3) and (4.4). Even in this case (which, note, has measure zero in parameter space), we see that combination of BigBOSS and Planck is extremely beneficial.[5]

5   Conclusions

This paper focused on the ability of upcoming LSS and CMB surveys to probe more general models of primordial non-Gaussianity. We concentrated in particular on the generalized local model where the parameter $f_{\rm NL}$ is promoted to an arbitrary function of scale $f_{\rm NL}(k)$. Our starting point were the piecewise constant parameters in k, constraints on which are shown in figure 2, and their principal components which are shown in figure 3 and constrained in figure 4.

---

[4]We performed our bias calculations in the Lagrangian picture where the primordial fluctuations are linearly extrapolated to $z = 0$ as usually done in the literature. For an alternative approach including the higher order corrections in the framework of the integrated perturbation theory, see ref. [68].

[5]While it may seem surprising that constraints away from the pivot wavenumber are finite given that $\sigma(n_{f_{\rm NL}}) = \infty$, we remind the reader that the infinite running of $f_{\rm NL}(k)$ is essentially multiplied with zero amplitude $f_{\rm NL}^*$ when calculating the constraints at the fiducial value $f_{\rm NL}(k) = 0$. Closer inspection of eqs. (4.3) and (4.4) confirms this argument.

Comparison with theory is easiest, however, by using a simpler parametrization in terms of "running" of the spectral index, $n_{f_{\rm NL}} \equiv d \ln f_{\rm NL}(k)/d \ln k$. Using the two-parameter description of non-Gaussianity in terms of amplitude $f_{\rm NL}^*$ and running $n_{f_{\rm NL}}$, we studied the extent to which a combination of LSS and CMB observations can constrain the running (table 1) and $f_{\rm NL}(k)$ as a whole (figures 5, 6, and 7).

For the power-law $f_{\rm NL}(k)$, we found that both the bispectrum measurement from the CMB Planck survey and power spectrum measurement from an LSS survey can constrain $f_{\rm NL}(k)$ tightly in a relatively narrow range of wavenumbers around $k \simeq 0.1 h\,{\rm Mpc}^{-1}$. The scale best constrained by the CMB is larger (i.e. at a smaller k) than the scale best constrained by LSS: we get complementary information about $f_{\rm NL}(k)$ from the two data sets. The ability of LSS to constrain $f_{\rm NL}(k)$ effectively at a wide range of scales depends on the survey parameters and the fiducial model of $f_{\rm NL}(k)$ chosen, as is clear from figures 5–7 and table 2. Nonetheless, large galaxy redshift surveys planned for the future may well be competitive with, or even better than, the constraints on the magnitude and running of $f_{\rm NL}(k)$ expected from Planck.

Beyond the simple power-law model, we find that the combination of CMB and LSS helps pin down the best-constrained few principal components of $f_{\rm NL}(k)$ better than either probe alone. Figure 4 shows that the degree of complementarity significantly depends on the details of (and systematics in) the LSS survey.

The constraints from the DES and BigBOSS, and other upcoming LSS surveys can turn out to be worse *or better* than those illustrated here, depending on how well the systematics can be controlled. While (for example) the photometric redshift errors [28], calibration errors [69], and assembly bias of galaxies [70] can all introduce parameter biases and degrade constraints, accurate calibration of these effects from simulations and observations, as well as selection of the "golden" class of objects with well understood properties whose clustering to use to measure non-Gaussianity, can cancel out these degradations. Moreover, we have not considered information from the LSS *bispectrum* which, while somewhat notoriously difficult to theoretically estimate due to non-Gaussian contributions from the gravitational collapse at late times (though see [71, 72] for recent progress on the matter), is nevertheless a very potent probe of primordial non-Gaussianity (e.g. [48, 73–75]).

Overall, a full exploration of the LSS and CMB systematics is a herculean task beyond the scope of this paper; nevertheless, we think we captured a few key systematics with our choice of survey specifications and nuisance parameters.

Finally, we introduced the figure of merit for measurements of non-Gaussianity, defined as the inverse area of the constraint region in the plane of non-Gaussian amplitude and running (see eq. (4.5)). We are very encouraged by the fact that future constraints of non-Gaussianity will improve current-data figure of merit [67] by more than an order of magnitude, and thus shed interesting constraints on the physics of inflation.

Acknowledgments

A   Calculating the CMB bispectrum

Calculating the CMB bispectrum is a problem that has been well-studied elsewhere in the literature, both for the general case and primordial local non-Gaussianity (e.g. [3]). Here, we briefly review the technique for calculating the bispectrum in the case of local non-Gaussianity, as well as the extension to the generalized local model that we discuss in this paper.

The bispectrum is defined as:

$$B_{\ell_1\ell_2\ell_3,m_1m_2m_3} \equiv \langle a_{\ell_1 m_1} a_{\ell_2 m_2} a_{\ell_3 m_3} \rangle \tag{A.1}$$

where the $a_{\ell m}$s are the coefficients on the spherical harmonic decomposition of the CMB sky. The $a_{\ell m}$s can be related to the Bardeen curvature perturbations $\Phi(\mathbf{k})$ by:

$$a_{\ell m} = \int d^2\hat{\mathbf{k}} \, \frac{\Delta T(\hat{\mathbf{k}})}{T} Y^*_{\ell m}(\hat{\mathbf{k}}) = 4\pi(-i)^\ell \int \frac{d^3k}{(2\pi)^3} \, \Phi(\mathbf{k}) g_\ell(k) Y^*_{\ell m}(\hat{\mathbf{k}}) \tag{A.2}$$

Here, $g_\ell(k)$ is the CMB temperature radiation transfer function. There are several conventions used for this transfer function; $g_\ell(k)$ is related to the transfer function $T_\ell(k)$ found in [77] by:

$$g_\ell(k) = \frac{(-i)^\ell}{\sqrt{2\ell(\ell+1)}} T_\ell(k) \tag{A.3}$$

Throughout this paper, we denote the radiation transfer functions as $t_\ell(k)$, defined as:

$$t_\ell(k) = \frac{1}{(-i)^\ell} g_\ell(k) = \frac{1}{\sqrt{2\ell(\ell+1)}} T_\ell(k) \tag{A.4}$$

With these transfer functions, (A.2) becomes:

$$a_{\ell m} = \frac{4\pi}{\sqrt{2\ell(\ell+1)}}(-1)^\ell \int \frac{d^3k}{(2\pi)^3} \, \Phi(\mathbf{k}) t_\ell(k) Y^*_{\ell m}(\hat{\mathbf{k}}). \tag{A.5}$$

The angular-averaged bispectrum $B_{\ell_1\ell_2\ell_3}$ is related to the raw bispectrum $B_{\ell_1\ell_2\ell_3,m_1m_2m_3}$ of (A.1) by the relation:

$$B_{\ell_1\ell_2\ell_3} = \sum_{m_1,m_2,m_3} \begin{pmatrix} \ell_1 & \ell_2 & \ell_3 \\ m_1 & m_2 & m_3 \end{pmatrix} B_{\ell_1\ell_2\ell_3,m_1m_2m_3}. \tag{A.6}$$

Here, $\begin{pmatrix} \ell_1 & \ell_2 & \ell_3 \\ m_1 & m_2 & m_3 \end{pmatrix}$ is the Wigner 3j-symbol.[6] Substituting (A.1) and (A.5) into (A.6), we obtain the following expression for the angular-averaged bispectrum:

$$B_{\ell_1\ell_2\ell_3} = (4\pi)^3(-1)^{\ell_1+\ell_2+\ell_3} \sum_{m_1,m_2,m_3} \begin{pmatrix} \ell_1 & \ell_2 & \ell_3 \\ m_1 & m_2 & m_3 \end{pmatrix} \int \frac{d^3k_1}{(2\pi)^3} \frac{d^3k_2}{(2\pi)^3} \frac{d^3k_3}{(2\pi)^3}$$
$$\times Y^*_{\ell_1 m_1}(\hat{\mathbf{k_1}}) Y^*_{\ell_2 m_2}(\hat{\mathbf{k_2}}) Y^*_{\ell_3 m_3}(\hat{\mathbf{k_3}}) t_{\ell_1}(k_1) t_{\ell_2}(k_2) t_{\ell_3}(k_3) \langle \Phi(\mathbf{k_1}) \Phi(\mathbf{k_2}) \Phi(\mathbf{k_3}) \rangle. \tag{A.7}$$

Using the definition of the Bardeen curvature bispectrum, B_Φ,

$$\langle \Phi(\mathbf{k_1}) \Phi(\mathbf{k_2}) \Phi(\mathbf{k_3}) \rangle = (2\pi)^3 \delta(\mathbf{k_1} + \mathbf{k_2} + \mathbf{k_3}) B_\Phi(k_1, k_2, k_3), \tag{A.8}$$

---

[6]There are some computational difficulties that arise when evaluating the 3j-symbol for high $l_{1,2,3}$; see appendix D.2 for more on this.

we find

$$B_{\ell_1 \ell_2 \ell_3} = \frac{1}{\pi^3} \sum_{m_1, m_2, m_3} \begin{pmatrix} \ell_1 & \ell_2 & \ell_3 \\ m_1 & m_2 & m_3 \end{pmatrix} \int d^3 k_1 \, d^3 k_2 \, d^3 k_3 Y^*_{\ell_1 m_1}(\hat{\mathbf{k_1}}) Y^*_{\ell_2 m_2}(\hat{\mathbf{k_2}}) Y^*_{\ell_3 m_3}(\hat{\mathbf{k_3}})$$

$$\times t_{\ell_1}(k_1) t_{\ell_2}(k_2) t_{\ell_3}(k_3) \delta(\mathbf{k_1} + \mathbf{k_2} + \mathbf{k_3}) B_\Phi(k_1, k_2, k_3). \tag{A.9}$$

(The prefactor of $(-1)^{\ell_1 + \ell_2 + \ell_3}$ vanished because the Wigner 3j-symbol ensures $\ell_1 + \ell_2 + \ell_3$ is even.) Taking advantage of several identities in [78] (their (12) and (13)), the orthogonality of the spherical harmonics, and the Gaunt integral identity ([8]), this becomes:

$$B_{\ell_1 \ell_2 \ell_3} = \left(\frac{2}{\pi}\right)^3 I_{\ell_1 \ell_2 \ell_3} \int k_1^2 dk_1 \, k_2^2 dk_2 \, k_3^2 dk_3 B_\Phi(k_1, k_2, k_3) t_{\ell_1}(k_1) t_{\ell_2}(k_2) t_{\ell_3}(k_3)$$

$$\times \int_0^\infty r^2 dr \, j_{\ell_1}(k_1 r) j_{\ell_2}(k_2 r) j_{\ell_3}(k_3 r), \tag{A.10}$$

where $I_{\ell_1 \ell_2 \ell_3}$ is the Gaunt integral

$$I_{\ell_1 \ell_2 \ell_3} = \sqrt{\frac{(2\ell_1 + 1)(2\ell_2 + 1)(2\ell_3 + 1)}{4\pi}} \begin{pmatrix} \ell_1 & \ell_2 & \ell_3 \\ 0 & 0 & 0 \end{pmatrix}. \tag{A.11}$$

The real-space integral is now a one-dimensional integral in the spherical coordinate r, starting at our location and ending at infinity. This real-space coordinate is the difference in the conformal time $\Delta\eta = \int_{t_e}^{t_0} \frac{dt}{a} = c(\tau_0 - \tau_e)$ between the time when the CMB was emitted and the present. Nearly all of the contribution to the integral in r comes from a short period of time around the surface of last scattering, and there are no physical contributions beyond $r > r_{\max} = \eta_0 = c\tau_0 \approx 14.6$ Gpc. To perform this integral, we sampled it 150 times between $r_{\max}$ and $r_{\max} - 2r_*$, where $r_{\max} - r_*$ is the comoving distance to the surface of last scattering. We also sampled 50 times between $r_{\max} - 2r_*$ and 0 to capture any impact that late-time effects might have had. Increasing the sampling rate did not significantly improve our results.

A.1 Derivatives with respect to f_{NL} and $f_{\mathrm{NL}}(k)$

Using (A.10) along with (3.3), we get the following expression for the angular-averaged CMB bispectrum in the constant f_{NL} case:

$$B_{\ell_1 \ell_2 \ell_3} = 2\Delta_\phi^2 f_{\mathrm{NL}} \left(\frac{2}{\pi}\right)^3 I_{\ell_1 \ell_2 \ell_3} \int k_1^2 dk_1 \, k_2^2 dk_2 \, k_3^2 dk_3 \left(\frac{1}{k_1^{3-(n_s-1)} k_2^{3-(n_s-1)}} + \mathrm{perm.}\right)$$

$$\times t_{\ell_1}(k_1) t_{\ell_2}(k_2) t_{\ell_3}(k_3) \int_0^\infty r^2 dr \, j_{\ell_1}(k_1 r) j_{\ell_2}(k_2 r) j_{\ell_3}(k_3 r). \tag{A.12}$$

Following [5, 8] we define functions $\alpha_\ell(r)$ and $\beta_\ell(r)$ to help us rewrite (A.12) as

$$\alpha_\ell(r) \equiv \frac{2}{\pi} \int k^2 t_\ell(k) j_\ell(kr) dk \tag{A.13}$$

$$\beta_\ell(r) \equiv \frac{2}{\pi} \int k^{-(2-n_s)} t_\ell(k) j_\ell(kr) dk. \tag{A.14}$$

Now eq. (A.12) reads

$$B_{\ell_1 \ell_2 \ell_3} = 2\Delta_\phi^2 f_{\mathrm{NL}} I_{\ell_1 \ell_2 \ell_3} \int_0^\infty r^2 dr \left(\alpha_{\ell_1}(r) \beta_{\ell_2}(r) \beta_{\ell_3}(r) + \mathrm{perm.}\right) \tag{A.15}$$

– 17 –

and hence

$$\frac{\partial B_{\ell_1\ell_2\ell_3}}{\partial f_{\rm NL}} = \frac{1}{f_{\rm NL}}B_{\ell_1\ell_2\ell_3}. \tag{A.16}$$

For the scale-*dependent* $f_{\rm NL}(k)$ case, we use (3.5) to find that the angular-averaged CMB bispectrum is:

$$\frac{\partial B_{\ell_1\ell_2\ell_3}}{\partial f_{\rm NL}^i} = 2\Delta_\phi^2 I_{\ell_1\ell_2\ell_3} \int_0^\infty r^2 dr \left(\alpha_{\ell_1}^i(r)\beta_{\ell_2}(r)\beta_{\ell_3}(r) + \text{perm.}\right) \tag{A.17}$$

where

$$\alpha_\ell^i(r) \equiv \frac{2}{\pi} \int_{k_i^{\rm lower}}^{k_i^{\rm upper}} k^2 t_\ell(k) j_\ell(kr) dk. \tag{A.18}$$

A.2 Polarization and cross-terms

The bispectrum for multiple fields is a simple extension of the single field case. By analogy with eqs. (A.1) and (A.2), the multiple-field bispectrum is

$$B_{\ell_1\ell_2\ell_3,m_1m_2m_3}^{pqr} = \langle a_{\ell_1 m_1}^p a_{\ell_2 m_2}^q a_{\ell_3 m_3}^r \rangle, \tag{A.19}$$

where

$$a_{\ell m}^p = \frac{4\pi}{\sqrt{2\ell(\ell+1)}}(-1)^\ell \int \frac{d^3k}{(2\pi)^3} \, \Phi(\mathbf{k})t_\ell^p(k)Y_{\ell m}^*(\hat{\mathbf{k}}) \tag{A.20}$$

and $t_\ell^i(k)$ is either the temperature or polarization radiation transfer function. Using these definitions and running through eqs. (A.7) through (A.17) again, we can rewrite the bispectrum for multiple fields if we just modify eqs. (A.13), (A.14), and (A.18) slightly:

$$\alpha_\ell^p(r) \equiv \frac{2}{\pi} \int k^2 t_\ell^p(k) j_\ell(kr) dk; \tag{A.21}$$

$$\beta_\ell^p(r) \equiv \frac{2}{\pi} \int k^{-(2-n_s)} t_\ell^p(k) j_\ell(kr) dk; \tag{A.22}$$

$$\alpha_\ell^{p,i}(r) \equiv \frac{2}{\pi} \int_{k_i^{\rm lower}}^{k_i^{\rm upper}} k^2 t_\ell^p(k) j_\ell(kr) dk. \tag{A.23}$$

So for the constant $f_{\rm NL}$ case, we have

$$\frac{\partial B_{\ell_1\ell_2\ell_3}^{pqr}}{\partial f_{\rm NL}} = 2\Delta_\phi^2 I_{\ell_1\ell_2\ell_3} \int_0^\infty r^2 dr \left(\alpha_{\ell_1}^p(r)\beta_{\ell_2}^q(r)\beta_{\ell_3}^r(r) + \text{perm.}\right), \tag{A.24}$$

while for the piecewise-constant $f_{\rm NL}(k)$ case, we have:

$$\frac{\partial B_{\ell_1\ell_2\ell_3}^{pqr}}{\partial f_{\rm NL}^i} = 2\Delta_\phi^2 I_{\ell_1\ell_2\ell_3} \int_0^\infty r^2 dr \left(\alpha_{\ell_1}^{p,i}(r)\beta_{\ell_2}^q(r)\beta_{\ell_3}^r(r) + \text{perm.}\right). \tag{A.25}$$

B The covariance of the bispectrum

It is usually a good assumption to consider only the Gaussian contribution to the covariance of the bispectrum, $\mathbf{C}$. Using Wick's theorem, one can straightforwardly show ([4, 57, 58]):

$$\mathbf{C}_{\ell_1\ell_2\ell_3} = C_{\ell_1} C_{\ell_2} C_{\ell_3} \tag{B.1}$$

where

$$C_\ell = C_\ell^{CV} + \sigma_\ell^2 W_\ell = C_\ell^{CV} + C_\ell^N, \tag{B.2}$$

where C_ℓ^{CV} is cosmic variance, while C_ℓ^N is the variance due to the noise and beam width in the survey; moreover, σ_ℓ^2 is the variance of the noise in the survey per pixel, and W_ℓ is a "window" term relating to the survey beam type and width ([79, 80]).[7] For an experiment with multiple frequency channels (such as Planck or WMAP), the basic form of equation (B.2) still holds, but finding C_ℓ^N is slightly trickier ([79]):

$$\frac{1}{C_\ell^N} = \sum_\nu \frac{1}{C_\ell^N(\nu)} = \sum_\nu \frac{1}{\sigma_\ell^2(\nu) W_\ell(\nu)}. \tag{B.3}$$

For uncorrelated Gaussian noise, $\sigma_\ell^2(\nu) = \sigma^2(\nu)$ is constant, and we can find its value for a particular experiment — for example, the Planck beam width and noise parameters are found in the Planck mission "blue book."

We have only been dealing with temperature (TT), but it is not significantly harder to add in polarization (EE) and cross (TE) terms. The covariance matrix here is ([21, 57])

$$(\mathbf{C}_{\ell_1\ell_2\ell_3}^{-1})_{lmn,pqr} = (C_{\ell_1}^{-1})_{lp}(C_{\ell_2}^{-1})_{mq}(C_{\ell_3}^{-1})_{nr}, \tag{B.4}$$

where

$$C_\ell = \begin{pmatrix} C_\ell^{TT} & C_\ell^{TE} \\ C_\ell^{TE} & C_\ell^{EE} \end{pmatrix}. \tag{B.5}$$

Noise is dealt with in the same way as in (B.2) for C_ℓ^{TT} and C_ℓ^{EE} in (B.5). Assuming that the noise for T and E are uncorrelated, $\sigma_{TE}^2 = \langle \Delta T \Delta E \rangle = \langle \Delta T \rangle \langle \Delta E \rangle = 0$, and thus $C_\ell^{N,TE} = 0$ for all ℓ.

C The high-peak limit

Desjacques et al. [33] have identified a new term that contributes to the scale-dependent bias due to non-Gaussianity, which becomes important when the high-peak limit assumption is relaxed. This new term successfully explains previously mysterious discrepancies [14] between the theoretical expectation for the scale-dependent bias and the results of numerical simulations. Physically, the new term accounts for the scale-dependent mapping between the interval in the peak height $d\nu$ (which is featured in the peak-background split derivation of the bias) and mass interval dM.

Moreover, this term is only non-zero for cases when $f_{\rm NL} \neq$ const, and therefore it affects constraints on $f_{\rm NL}(k)$ that we study in this paper, but not the numerous forecasts for constant $f_{\rm NL}$ studied previously in the literature.

The new term corresponds to the second term of eq. (2.3)

$$N(k) \equiv \frac{d \ln F(k)}{d \ln \sigma_R}. \tag{C.1}$$

We can make the evaluation of this term more tractable by using the chain rule

$$N(k) = \frac{\sigma_R}{F(k)} \frac{dF}{dM} \left(\frac{d\sigma_R}{dM} \right)^{-1}. \tag{C.2}$$

---

[7]Note that [79] uses w^{-1} for what we are calling σ^2.

Now we will need to take the derivative of $N(k)$ with respect to the $f_{\rm NL}^i$, for our Fisher matrix.

$$\frac{\partial N}{\partial f_{\rm NL}^i} = \sigma_R \left(\frac{d\sigma_R}{dM}\right)^{-1} \frac{\partial}{\partial f_{\rm NL}^i} \left[\frac{1}{F(k)}\frac{dF}{dM}\right]$$
$$= \frac{\sigma_R}{F}\left(\frac{d\sigma_R}{dM}\right)^{-1} \frac{\partial}{\partial f_{\rm NL}^i}\left[\frac{d}{dM}\left(\frac{\partial F}{\partial f_{\rm NL}^i}\right) - \frac{1}{F}\frac{dF}{dM}\frac{\partial F}{\partial f_{\rm NL}^i}\right]. \tag{C.3}$$

Equations (C.2) and (C.3) are everything we need to properly account for the new term in our Fisher matrix. Note that σ_R and $d\sigma_R/dM$ are the only redshift-dependent quantities in $N(k)$; since their redshift dependence is linear and exactly the same, it cancels entirely, leaving $N(k)$ independent of z.

The effect of this new term on the projected constraints for the $f_{\rm NL}^i$, with a fiducial value of $f_{\rm NL}^i = 30$, are seen in figure 8. The figure illustrates that this new term removes much of the correlation between errors in neighboring $f_{\rm NL}^i$ and slightly broadens the range of scales at which the survey is sensitive to $f_{\rm NL}(k)$. Nevertheless, given that we are expanding our general $f_{\rm NL}(k)$ model around a constant value (30 or zero), the effects of this new term on the constraints on the amplitude and running of $f_{\rm NL}$ — $f_{\rm NL}^*$ and $n_{f_{\rm NL}}$ — are small.

D   Calculational details

D.1 ℓ sampling and binning

In evaluating equation (3.7), we do not actually use every $\ell \leq \ell_{\rm max}$; that would be incredibly computationally expensive. Instead, we sample and bin in ℓ. We keep every ℓ up through $\ell = 40$, at which point sampling drops off gradually until, at $\ell \gtrsim 100$, only every tenth ℓ is sampled. The "width" of the bins in ℓ are given by the equation

$$\Delta_{\ell_i} = \frac{1}{2}\left[(\ell_i - \ell_{i-1}) + (\ell_{i+1} - \ell_i)\right] = \frac{1}{2}(\ell_{i+1} - \ell_{i-1}). \tag{D.1}$$

D.2   Calculating the Wigner $3j$-symbol

We need to be able to calculate the Wigner $3j$-symbol for large (> 1000) values of $\ell_{1,2,3}$ in order to evaluate many of the expressions we're interested in. Unfortunately, the $3j$ function built in to the GNU Scientific Library can't properly evaluate the symbol for $\ell_{1,2,3} \gtrsim 70$. Thus, we were forced to create our own special-purpose $3j$-evaluator. Thankfully, we're only interested in the special case $m_{1,2,3} = 0$; as it turns out, in this case, the $3j$-symbol reduces to (see Wolfram Mathworld: http://mathworld.wolfram.com/Wigner3j-Symbol.html):

$$\begin{pmatrix} \ell_1 & \ell_2 & \ell_3 \\ 0 & 0 & 0 \end{pmatrix} = \begin{cases} (-1)^g \sqrt{\frac{(2g-2\ell_1)!(2g-2\ell_2)!(2g-2\ell_3)!}{(2g+1)!}} \frac{g!}{(g-\ell_1)!(g-\ell_2)!(g-\ell_3)!} & \text{if } L = 2g; \\ 0 & \text{if } L = 2g+1, \end{cases} \tag{D.2}$$

where $L = \ell_1 + \ell_2 + \ell_3$. Since (D.2) involves evaluating the factorials of relatively large numbers when any of $l_{1,2,3}$ are large, we used Stirling's approximation to perform the factorials — but we needed the factorials to remain accurate even when the arguments were small, so we used six terms in the approximation.
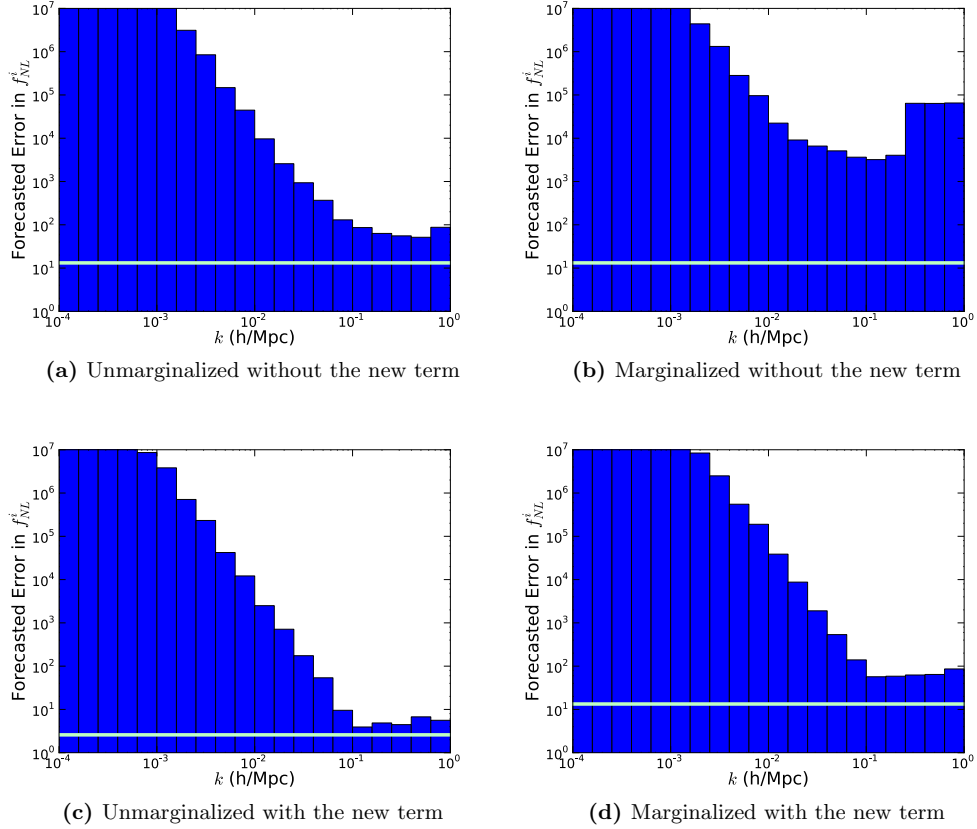
(a) Unmarginalized without the new term

(b) Marginalized without the new term

(c) Unmarginalized with the new term

(d) Marginalized with the new term

Figure 8. Illustration of how the inclusion of the correction to the scale-dependent bias from [33] affects the forecasted constraints on the f_{NL}^i from DES. For comparison, the green line is the constraint found for a constant f_{NL} using the same assumptions.

References

[1] X. Chen, *Primordial non-Gaussianities from inflation models*, *Adv. Astron.* **2010** (2010) 638979 [arXiv:1002.1416] [INSPIRE].

[2] E. Komatsu, *Hunting for primordial non-Gaussianity in the cosmic microwave background*, *Class. Quant. Grav.* **27** (2010) 124010 [arXiv:1003.6097] [INSPIRE].

[3] N. Bartolo, E. Komatsu, S. Matarrese and A. Riotto, *Non-Gaussianity from inflation: theory and observations*, *Phys. Rept.* **402** (2004) 103 [astro-ph/0406398] [INSPIRE].

[4] M. Liguori, E. Sefusatti, J. Fergusson and E. Shellard, *Primordial non-Gaussianity and bispectrum measurements in the cosmic microwave background and large-scale structure*, *Adv. Astron.* **2010** (2010) 980523 [arXiv:1001.4707] [INSPIRE].

[5] A.P. Yadav and B.D. Wandelt, *Primordial non-Gaussianity in the cosmic microwave background*, *Adv. Astron.* **2010** (2010) 565248 [arXiv:1006.0275] [INSPIRE].

[6] D. Salopek and J. Bond, *Nonlinear evolution of long wavelength metric fluctuations in inflationary models*, *Phys. Rev.* **D 42** (1990) 3936 [INSPIRE].

[7] L. Verde, L.-M. Wang, A. Heavens and M. Kamionkowski, *Large scale structure, the cosmic microwave background and primordial non-Gaussianity*, *Mon. Not. Roy. Astron. Soc.* **313** (2000) L141 [astro-ph/9906301] [INSPIRE].

[8] E. Komatsu and D.N. Spergel, *Acoustic signatures in the primary microwave background bispectrum*, *Phys. Rev.* **D 63** (2001) 063002 [astro-ph/0005036] [INSPIRE].

[9] M. Liguori, S. Matarrese and L. Moscardini, *High-resolution simulations of cosmic microwave background non-Gaussian maps in spherical coordinates*, *Astrophys. J.* **597** (2003) 57 [astro-ph/0306248] [INSPIRE].

[10] D. Babich, P. Creminelli and M. Zaldarriaga, *The shape of non-Gaussianities*, *JCAP* **08** (2004) 009 [astro-ph/0405356] [INSPIRE].

[11] A. Becker, D. Huterer and K. Kadota, *Scale-dependent non-Gaussianity as a generalization of the local model*, *JCAP* **01** (2011) 006 [arXiv:1009.4189] [INSPIRE].

[12] R. Bean, X. Chen, H. Peiris and J. Xu, *Comparing infrared Dirac-Born-Infeld brane inflation to observations*, *Phys. Rev.* **D 77** (2008) 023527 [arXiv:0710.1812] [INSPIRE].

[13] C.T. Byrnes, M. Gerstenlauer, S. Nurmi, G. Tasinato and D. Wands, *Scale-dependent non-Gaussianity probes inflationary physics*, *JCAP* **10** (2010) 004 [arXiv:1007.4277] [INSPIRE].

[14] S. Shandera, N. Dalal and D. Huterer, *A generalized local ansatz and its effect on halo bias*, *JCAP* **03** (2011) 017 [arXiv:1010.3722] [INSPIRE].

[15] N. Barnaby, R. Namba and M. Peloso, *Phenomenology of a pseudo-scalar inflaton: naturally large non-Gaussianity*, *JCAP* **04** (2011) 009 [arXiv:1102.4333] [INSPIRE].

[16] PLANCK collaboration, *The scientific programme of Planck*, astro-ph/0604069 [INSPIRE].

[17] E. Sefusatti, M. Liguori, A.P. Yadav, M.G. Jackson and E. Pajer, *Constraining running non-Gaussianity*, *JCAP* **12** (2009) 022 [arXiv:0906.0232] [INSPIRE].

[18] T. Giannantonio, C. Porciani, J. Carron, A. Amara and A. Pillepich, *Constraining primordial non-Gaussianity with future galaxy surveys*, *Mon. Not. Roy. Astron. Soc.* **422** (2012) 2854 [arXiv:1109.0958] [INSPIRE].

[19] E. Sefusatti, C. Vale, K. Kadota and J. Frieman, *Primordial non-Gaussianity and dark energy constraints from cluster surveys*, *Astrophys. J.* **658** (2007) 669 [astro-ph/0609124] [INSPIRE].

[20] K.M. Smith and M. Zaldarriaga, *Algorithms for bispectra: forecasting, optimal analysis and simulation*, *Mon. Not. Roy. Astron. Soc.* **417** (2011) 2 [astro-ph/0612571] [INSPIRE].

[21] A.P. Yadav, E. Komatsu and B.D. Wandelt, *Fast estimator of primordial non-Gaussianity from temperature and polarization anisotropies in the cosmic microwave background*, *Astrophys. J.* **664** (2007) 680 [astro-ph/0701921] [INSPIRE].

[22] P. McDonald, *Primordial non-Gaussianity: large-scale structure signature in the perturbative bias model*, *Phys. Rev.* **D 78** (2008) 123519 [arXiv:0806.1061] [INSPIRE].

[23] C. Carbone, L. Verde and S. Matarrese, *Non-Gaussian halo bias and future galaxy surveys*, *Astrophys. J.* **684** (2008) L1 [arXiv:0806.1950] [INSPIRE].

[24] A. Slosar, *Optimal dataset combining in f_{NL} constraints from large scale structure*, *JCAP* **03** (2009) 004 [arXiv:0808.0044] [INSPIRE].

[25] C. Carbone, O. Mena and L. Verde, *Cosmological parameters degeneracies and non-Gaussian halo bias*, *JCAP* **07** (2010) 020 [arXiv:1003.0456] [INSPIRE].

[26] J.R. Fergusson, M. Liguori and E.P.S. Shellard, *General CMB and primordial bispectrum estimation: mode expansion, map making, and measures of f_{NL}*, *Phys. Rev.* **D 82** (2010) 023502 [arXiv:0912.5516] [INSPIRE].

[27] B. Sartoris et al., *The potential of X-ray cluster surveys to constrain primordial non-Gaussianity*, *Mon. Not. Roy. Astron. Soc.* **407** (2010) 2339 [arXiv:1003.0841] [INSPIRE].

[28] C. Cunha, D. Huterer and O. Doré, *Primordial non-Gaussianity from the covariance of galaxy cluster counts*, *Phys. Rev.* **D 82** (2010) 023004 [arXiv:1003.2416] [INSPIRE].

[29] C. Fedeli, C. Carbone, L. Moscardini and A. Cimatti, *The clustering of galaxies and galaxy clusters: constraints on primordial non-Gaussianity from future wide-field surveys*, *Mon. Not. Roy. Astron. Soc.* **414** (2011) 1545 [arXiv:1012.2305] [INSPIRE].

[30] S. Joudaki, O. Dore, L. Ferramacho, M. Kaplinghat and M.G. Santos, *Primordial non-Gaussianity from the* 21 *cm power spectrum during the epoch of reionization*, *Phys. Rev. Lett.* **107** (2011) 131304 [arXiv:1105.1773] [INSPIRE].

[31] A. Pillepich, C. Porciani and T.H. Reiprich, *The X-ray cluster survey with eROSITA: forecasts for cosmology, cluster physics and primordial non-Gaussianity*, *Mon. Not. Roy. Astron. Soc.* **422** (2012) 44 [arXiv:1111.6587] [INSPIRE].

[32] D.K. Hazra and T.G. Sarkar, *Primordial non-Gaussianity in the forest:* 3D *bispectrum of Ly-α flux spectra along multiple lines of sight*, *Phys. Rev. Lett.* **109** (2012) 149902 [arXiv:1205.2790] [INSPIRE].

[33] V. Desjacques, D. Jeong and F. Schmidt, *Accurate predictions for the scale-dependent galaxy bias from primordial non-Gaussianity*, *Phys. Rev.* **D 84** (2011) 061301 [arXiv:1105.3476] [INSPIRE].

[34] N. Dalal, O. Doré, D. Huterer and A. Shirokov, *The imprints of primordial non-Gaussianities on large-scale structure: scale dependent bias and abundance of virialized objects*, *Phys. Rev.* **D 77** (2008) 123514 [arXiv:0710.4560] [INSPIRE].

[35] S. Matarrese and L. Verde, *The effect of primordial non-Gaussianity on halo bias*, *Astrophys. J.* **677** (2008) L77 [arXiv:0801.4826] [INSPIRE].

[36] M. Grossi, K. Dolag, E. Branchini, S. Matarrese and L. Moscardini, *Evolution of massive haloes in non-Gaussian scenarios*, *Mon. Not. Roy. Astron. Soc.* **382** (2007) 1261 [arXiv:0707.2516] [INSPIRE].

[37] A. Slosar, C. Hirata, U. Seljak, S. Ho and N. Padmanabhan, *Constraints on local primordial non-Gaussianity from large scale structure*, *JCAP* **08** (2008) 031 [arXiv:0805.3580] [INSPIRE].

[38] N. Afshordi and A.J. Tolley, *Primordial non-Gaussianity, statistics of collapsed objects and the Integrated Sachs-Wolfe effect*, *Phys. Rev.* **D 78** (2008) 123507 [arXiv:0806.1046] [INSPIRE].

[39] A. Taruya, K. Koyama and T. Matsubara, *Signature of primordial non-Gaussianity on matter power spectrum*, *Phys. Rev.* **D 78** (2008) 123534 [arXiv:0808.4085] [INSPIRE].

[40] V. Desjacques, U. Seljak and I. Iliev, *Scale-dependent bias induced by local non-Gaussianity: a comparison to N-body simulations*, *Mon. Not. Roy. Astron. Soc.* **396** (2009) 85 [arXiv:0811.2748] [INSPIRE].

[41] A. Pillepich, C. Porciani and O. Hahn, *Universal halo mass function and scale-dependent bias from N-body simulations with non-Gaussian initial conditions*, *Mon. Not. Roy. Astron. Soc.* **402** (2010) 191 [arXiv:0811.4176] [INSPIRE].

[42] P. Valageas, *Mass function and bias of dark matter halos for non-Gaussian initial conditions*, *Astron. Astrophys.* **514** (2010) A46 [arXiv:0906.1042] [INSPIRE].

[43] T. Giannantonio and C. Porciani, *Structure formation from non-Gaussian initial conditions: multivariate biasing, statistics and comparison with N-body simulations*, *Phys. Rev.* **D 81** (2010) 063530 [arXiv:0911.0017] [INSPIRE].

[44] F. Schmidt and M. Kamionkowski, *Halo clustering with non-local non-Gaussianity*, *Phys. Rev.* **D 82** (2010) 103002 [arXiv:1008.0638] [INSPIRE].

[45] V. Desjacques, D. Jeong and F. Schmidt, *Non-Gaussian halo bias re-examined: mass-dependent amplitude from the peak-background split and thresholding*, *Phys. Rev.* **D 84** (2011) 063512 [arXiv:1105.3628] [INSPIRE].

[46] C. Wagner, L. Verde and L. Boubekeur, *N-body simulations with generic non-Gaussian initial conditions I: power spectrum and halo mass function*, *JCAP* **10** (2010) 022 [arXiv:1006.5793] [INSPIRE].

[47] C. Wagner and L. Verde, *N-body simulations with generic non-Gaussian initial conditions II: halo bias*, *JCAP* **03** (2012) 002 [arXiv:1102.3229] [INSPIRE].

[48] E. Sefusatti, M. Crocce and V. Desjacques, *The halo bispectrum in N-body simulations with non-Gaussian initial conditions*, arXiv:1111.6966 [INSPIRE].

[49] B. Grinstein and M.B. Wise, *Non-Gaussian fluctuations and the correlations of galaxies or rich clusters of galaxies*, *Astrophys. J.* **310** (1986) 19 [INSPIRE].

[50] S. Matarrese, F. Lucchin and S.A. Bonometto, *A path integral approach to large scale matter distribution originated by non-Gaussian fluctuations*, *Astrophys. J.* **310** (1986) L21 [INSPIRE].

[51] M. Tegmark, *Measuring cosmological parameters with galaxy surveys*, *Phys. Rev. Lett.* **79** (1997) 3806 [astro-ph/9706198] [INSPIRE].

[52] H.-J. Seo and D.J. Eisenstein, *Probing dark energy with baryonic acoustic oscillations from future large galaxy redshift surveys*, *Astrophys. J.* **598** (2003) 720 [astro-ph/0307460] [INSPIRE].

[53] D. Schlegel et al., *The BigBOSS experiment*, arXiv:1106.1706 [INSPIRE].

[54] WMAP collaboration, E. Komatsu et al., *Seven-year Wilkinson Microwave Anisotropy Probe (WMAP) observations: cosmological interpretation*, *Astrophys. J. Suppl.* **192** (2011) 18 [arXiv:1001.4538] [INSPIRE].

[55] *Bigboss*, technical report, (2012).

[56] DARK ENERGY SURVEY collaboration, T. Abbott et al., *The dark energy survey*, astro-ph/0510346 [INSPIRE].

[57] D. Babich and M. Zaldarriaga, *Primordial bispectrum information from CMB polarization*, *Phys. Rev.* **D 70** (2004) 083005 [astro-ph/0408455] [INSPIRE].

[58] D.N. Spergel and D.M. Goldberg, *Microwave background bispectrum. 1. Basic formalism*, *Phys. Rev.* **D 59** (1999) 103001 [astro-ph/9811252] [INSPIRE].

[59] M. Liguori and A. Riotto, *Impact of uncertainties in the cosmological parameters on the measurement of primordial non-Gaussianity*, *Phys. Rev.* **D 78** (2008) 123004 [arXiv:0808.3255] [INSPIRE].

[60] X. Chen, *Running non-Gaussianities in DBI inflation*, *Phys. Rev.* **D 72** (2005) 123518 [astro-ph/0507053] [INSPIRE].

[61] M. LoVerde, A. Miller, S. Shandera and L. Verde, *Effects of scale-dependent non-Gaussianity on cosmological structures*, *JCAP* **04** (2008) 014 [arXiv:0711.4126] [INSPIRE].

[62] X. Chen, M.-X. Huang, S. Kachru and G. Shiu, *Observational signatures and non-Gaussianities of general single field inflation*, *JCAP* **01** (2007) 002 [hep-th/0605045] [INSPIRE].

[63] J. Khoury and F. Piazza, *Rapidly-varying speed of sound, scale invariance and non-Gaussian signatures*, *JCAP* **07** (2009) 026 [arXiv:0811.3633] [INSPIRE].

[64] C.T. Byrnes, K.-Y. Choi and L.M. Hall, *Large non-Gaussianity from two-component hybrid inflation*, *JCAP* **02** (2009) 017 [arXiv:0812.0807] [INSPIRE].

[65] A. Albrecht et al., *Report of the dark energy task force*, astro-ph/0609591 [INSPIRE].

[66] M.J. Mortonson, D. Huterer and W. Hu, *Figures of merit for present and future dark energy probes*, *Phys. Rev.* **D 82** (2010) 063004 [arXiv:1004.0236] [INSPIRE].

[67] A. Becker and D. Huterer, *First constraints on the running of non-Gaussianity*, *Phys. Rev. Lett.* **109** (2012) 121302 [arXiv:1207.5788] [INSPIRE].

[68] T. Matsubara, *Deriving an accurate formula of scale-dependent bias with primordial non-Gaussianity: an application of the integrated perturbation theory*, *Phys. Rev.* **D 86** (2012) 063518 [arXiv:1206.0562] [INSPIRE].

[69] D. Huterer, C.E. Cunha and W. Fang, *Calibration errors unleashed: effects on cosmological parameters and requirements for large-scale structure surveys*, arXiv:1211.1015 [INSPIRE].

[70] B.A. Reid, L. Verde, K. Dolag, S. Matarrese and L. Moscardini, *Non-Gaussian halo assembly bias*, *JCAP* **07** (2010) 013 [arXiv:1004.1637] [INSPIRE].

[71] K.C. Chan, R. Scoccimarro and R.K. Sheth, *Gravity and large-scale non-local bias*, *Phys. Rev.* **D 85** (2012) 083509 [arXiv:1201.3614] [INSPIRE].

[72] T. Baldauf, U. Seljak, V. Desjacques and P. McDonald, *Evidence for quadratic tidal tensor bias from the halo bispectrum*, *Phys. Rev.* **D 86** (2012) 083540 [arXiv:1201.4827] [INSPIRE].

[73] E. Sefusatti and E. Komatsu, *The bispectrum of galaxies from high-redshift galaxy surveys: primordial non-Gaussianity and non-linear galaxy bias*, *Phys. Rev.* **D 76** (2007) 083004 [arXiv:0705.0343] [INSPIRE].

[74] D. Jeong and E. Komatsu, *Primordial non-Gaussianity, scale-dependent bias and the bispectrum of galaxies*, *Astrophys. J.* **703** (2009) 1230 [arXiv:0904.0497] [INSPIRE].

[75] D. Figueroa, E. Sefusatti, A. Riotto and F. Vernizzi, *The effect of local non-Gaussianity on the matter bispectrum at small scales*, *JCAP* **08** (2012) 036 [arXiv:1205.2015] [INSPIRE].

[76] A. Lewis, A. Challinor and A. Lasenby, *Efficient computation of CMB anisotropies in closed FRW models*, *Astrophys. J.* **538** (2000) 473 [astro-ph/9911177] [INSPIRE].

[77] C. Gibelyou, D. Huterer and W. Fang, *Detectability of large-scale power suppression in the galaxy distribution*, *Phys. Rev.* **D 82** (2010) 123009 [arXiv:1007.0757] [INSPIRE].

[78] L.-M. Wang and M. Kamionkowski, *The cosmic microwave background bispectrum and inflation*, *Phys. Rev.* **D 61** (2000) 063504 [astro-ph/9907431] [INSPIRE].

[79] A.R. Cooray and W. Hu, *Imprint of reionization on the cosmic microwave background bispectrum*, *Astrophys. J.* **534** (2000) 533 [astro-ph/9910397] [INSPIRE].

[80] L. Knox, *Determination of inflationary observables by cosmic microwave background anisotropy experiments*, *Phys. Rev.* **D 52** (1995) 4307 [astro-ph/9504054] [INSPIRE].